Nanomedicine Journal

Received: Dec. 28, 2013; Accepted: Feb. 18, 2014
Vol. 1, No. 4, Summer 2014, page 238-247

Online ISSN 2322-5904
http://nmj.mums.ac.ir

Original Research

Study of magnetic and structural and optical properties of Zn doped Fe_3O_4 nanoparticles synthesized by co-precipitation method for biomedical application

Zahra Rezay Marand[1, 2*], Mitra Helmi Rashid Farimani[1, 2], Nasser Shahtahmasebi[1, 2]

[1]Department of physics, Faculty of Science, Ferdowsi University of Mashhad, Mashhad, Iran
[2]Nanoscience Center, Faculty of Science, Ferdowsi University of Mashhad, Mashhad, Iran

Abstract

Objective(s): This paper describes synthesizing of magnetic nanocomposite with co-precipitation method.
Materials and Methods: Magnetic $Zn_xFe_{3-x}O_4$ nanoparticles with 0-14% zinc doping (x=0, 0.025, 0.05, 0.075, 0.1 and 0.125) were successfully synthesized by co-precipitation method. The prepared zinc-doped Fe_3O_4 nanoparticles were characterized by X-ray diffraction (XRD), transmission electron microscopy (TEM), Fourier transform infrared spectroscopy (FTIR), vibrating sample magnetometer (VSM) and UV-Vis spectroscopy.
Results: results obtained from X-ray diffraction pattern have revealed the formation of single phase nanoparticles with cubic inverse spinal structures which size varies from 11.13 to 12.81 nm. The prepared nanoparticles have also possessed superparamagnetic properties at room temperature and high level of saturation magnetization with the maximum level of 74.60 emu/g for x=0.075. M_s changing in pure magnetite nanoparticles after impurities addition were explained based on two factors of "particles size" and "exchange interactions". Optical studies results revealed that band gaps in all Zn-doped NPs are higher than pure Fe_3O_4. As doping percent increases, band gap value decreases from 1.26 eV to 0.43 eV.
Conclusion: these magnetic nanocomposite structures since having superparamagnetic property offer a high potential for biosensing and biomedical application.

Keywords: Biomedical application, Fe_3O_4 nanoparticles, Saturation magnetization, Superparamagnetism, Zn-doping

***Corresponding Author:** *Zahra rezay marand, Department of physics, faculty of science, Ferdowsi University of Mashhad, Mashhad, Iran.*
Tel: +989125128605, Email: Zahra.rezaim.88@gmail.com

Introduction

During the last decade, nanosize magnetic materials have been largely studied due to their different magnetic properties compared to their bulk counterparts such as super-paramagnetism which can significantly advance the current clinical diagnostic and therapeutic methods (1). Each superparama-gnetic particle is a single magnetic domain in which thermal energy (K_BT) can overcome anisotropy energy barrier and cause free spin reversal. This is to say that no residual magnetism remains after elimination of external magnetic field.

In this regard, spinel ferrite nanocrystals with general chemical composition MFe_2O_4 (M= Co, Ni, Mn, Fe, Cu, Zn, etc.) form a group of applicable magnetic materials due to their interesting magnetic, magneto-resistive and magneto-optical properties (2). Among these materials, Fe_3O_4 or magnetite has attracted the most attention due to its unique magnetic and biomedical properties. Fe_3O_4 nanoparticles (NPs) offer a high potential of applications in many industrial and biological fields such as magnetic storage media, ferrofluids, magnetic refrig-eration, detoxification of biological fluids, magnetic cell separation, contrast agents in magnetic imaging (MRI), targeted drug delivery and hyperthermia treatment (3).

Magnetite with Fd3m space group has cubic inverse spinel structure in which oxygen anions have formed an fcc close packed structure and Fe cations have occupied interstitial tetrahedral and octahedral sites (4,5). In this structure, half of the Fe^{3+} ions are arranged in tetrahedral sites and the remaining half companied with all Fe^{2+} ions are arranged in octahedral sites. Based on the past reports, we might conclude that replacing Fe ions in interstitial sites with different metal ions such as Zn, Mn, Ga, Ni, Co and Cu will improve Fe_3O_4 unique physical properties originating from elec-trons hopping between Fe^{2+} and Fe^{3+} ions (6-9). Up to date, many approaches including thermal decomposition, microemulsion, hydrothermal, solvothermal,sonochemical, microwave assisted and co-precipitation have been developed for the preparation of Fe_3O_4 NPs (10). Among these methods, co-precipitation is most commonly method due to its advantages such as simple and cheap synthetic process, high yield product with superior magnetic and crystal properties and using inorganic reactant (11). In this research, at first, co-precipitation method has been used for synthesizing a set of Fe_3O_4 nanoparticles doped with Zn, represented as $Zn_xFe_{3-x}O_4$ (x=0-0.125), and then to investigate impurity effects on pure Fe_3O_4 NPs, we studied structural, magnetic and optical properties of samples by different characterization techniques.

Materials and Methods

Materials

Ferrous chloride tetrahydrate ($FeCl_2.4H_2O$), Ferric chloride hexahydrate ($FeCl_3.6H_2O$), Zinc chloride ($ZnCl_2$), hydrochloric acid (HCl), ammonium hydroxide (NH_4OH) and ethanol were purchased from Merck Co, and used without further purification. Deionized water was used at all experiment stages. Deionized water had been deoxygenated by bubbling N_2 gas.

Preparation of Fe_3O_4 nanoparticles

Fe_3O_4 nanoparticles doped with different amounts of Zinc demonstrated as $Zn_xFe_{3-x}O_4$ (x= 0, 0.025, 0.05, 0.075, 0.1 and 0.125) series were synthesized using chemical co-precipitation method. The typical procedure is as follows:

mentioned materials is produced. Then, NH_4OH solution (2 M, alkali source) in drops was added to the initial solution by vigorous magnetic stirring at 70°C. During this operation, the initial orange color of the solution turned to black as a result of magnetite NPs formation. After heating (for crystallizing structures), the resultant mag-netic precipitate was collected by applying an external magnetic field. Having been washed with ethanol and

water, it was dried under vacuum. It is worth mentioning that all main synthesis steps were performed under N_2 gas protection to create an oxygen-free atmosphere and prevent oxidation of divalent iron salts. Transmission electron microscope (TEM, LEO 912 AB) and Fourier transform infrared (FTIR) spectrophotometer (Avatar-370-FTIR Ther-monicolet) were also employed to characterization of Zn-doped Fe_3O_4 nano-particles. Magnetic measurements were carried out at room temperature by means of vibrating sample magnetometer (VSM). The UV-Vis absorption spectra of the nano-particles were measured by a UV-Vis spectrometer (LABOMET- 4057 UV-Vis).

Characterization

The phase purity and crystal structure of the samples were investigated using Philips PW1800 X-ray diffractometer (XRD) with Cu-K_α radiation (λ= 0.154 nm) and 0.04 degree step size.

Results and Discussion

Morphology and structure studies of the synthesized samples

Figure 1 demonstrates the XRD pattern of magnetite NPs doped with different amounts of Zn_x^{2+} (x= 0-0.125). As revealed, diffraction peaks of all samples completely correspond to standard pattern characteristic peaks of the magnetite cubic inverse spinel structure (JCPDS 19-0629). No secondary phase is detected to prove the formation of other Zn-based structures such as ZnO. So, we might conclude that Fe_3O_4 has been formed with high phase purity and Fe ions have been successfully replaced with Zn^{2+} ions.

To investigate effects of Zn doping on Fe_3O_4 NPs structural characteristics,

Debye-Scherrer formula (Eq. (1)) was used for calculating average crystalline size:

$$\mathbf{D_{XRD} = k\,\lambda / \beta\cos\theta} \qquad (1)$$

Where λ is the incident X-ray wavelength (1.54), θ is the Bragg diffraction angle, β (FWHM) is the radian-based full width at half-maximum and K is the grain shape factor (0.94) (12).

The average lattice constant value is calculated by Eq. (2) that is related to cubic structures:

$$\mathbf{a = d_{hkl}\,[h^2+k^2+l^2]^{1/2}} \qquad (2)$$

Where; l, k and h are Miller indexes and d_{hkl} is the distance between crystal planes ($d_{hkl} = \lambda / 2\sin\theta$) (13). Then, Williamson-Hale diagram (Eq. (3)) was implemented for estimating the amount of micro strain in crystal lattice (ε) (14):

$$\mathbf{\beta\cos\theta = k\lambda/D + 4\varepsilon\sin\theta} \qquad (3)$$

As shown in Figure 2 and Table 1 peak shift has occurred toward smaller angles in all $Zn_xFe_{3-x}O_4$ NPs, which has increased the distances between planes (311) and lattice constant.

This is mainly due to the large zinc ionic radius (74pm) compared to that of iron (64pm), which is predicted to expand crystal lattice (7), ε changes confirm this claim. Having replaced Zn in crystal lattice, ε value grew from minus value (indicting a contracting tension in pure Fe_3O_4 lattice x=0) to a positive value (indicting an expansive tension).

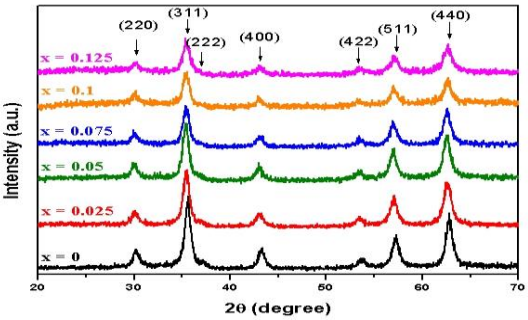

Figure 1. XRD pattern of Fe_3O_4 nanoparticles with different Zinc-doping percents.

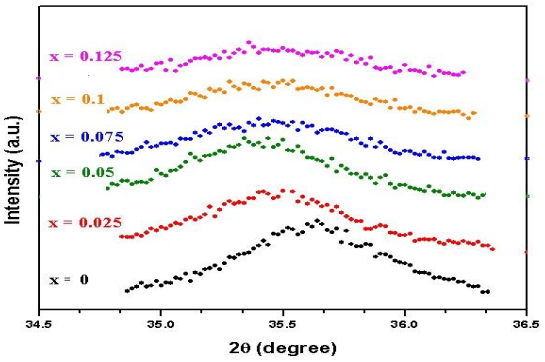

Figure 2. Magnifying the diffraction peak of (311) crystal planes.

Table 1. The obtained structural parameters of XRD analysis for (311) peak.

sample	2θ (˚)	FWHM (˚)	D_{XRD} (nm)	a (A˚)	d_{hkl} (A˚)	ε
x=0	35.61	0.689	12.65	8.324	2.518	-2.19×10^{-4}
x=0.025	35.46	0.788	11.13	8.382	2.528	$+2.32 \times 10^{-3}$
x=0.05	35.45	0.720	12.16	8.390	2.530	$+9.28 \times 10^{-4}$
x=0.075	35.39	0.684	12.81	8.401	2.533	$+1.04 \times 10^{-3}$
x=0.1	35.44	0.698	12.58	8.390	2.530	$+4.75 \times 10^{-3}$
x=0.125	35.43	0.697	12.58	8.393	2.531	$+1.63 \times 10^{-3}$

In addition to peak shift, doping has influenced and decreased diffraction peaks intensity Figure 2. That is to say that doping can decrease crystal order of Fe_3O_4 nanoparticles.

$Zn_xFe_{3-x}O_4$ nanoparticles TEM images with different Zn values are shown in Figure 3. As demonstrated, pure Fe_3O_4 nanoparticles have spherical shape and 5-25 nm size distribution with an average size of 14.29 nm. As Zn doping increases, Fe_3O_4 nanoparticles spherical morphology remains constant but their sizes change (Table 2). These changes trend corresponds to the results obtained from XRD analysis.

Magnetic properties analysis

To study synthesized NPs magnetic properties, magnetic measurements were performed at 300K temperature using VSM technique and *M-H* curves (magnetization changes due to applied external magnetic field) were depicted (Figure 4).

Based on the depicted curves, related data of initial magnetic susceptibility (χ_i), saturation magnetization (M_s), coercivity field (H_c) and remnant magnetization (M_r) were calculated as nanoparticles magnetic characteristics. Obtained results have been demonstrated in Table 3. The obtained results reveal that pure Fe_3O_4 NPs and Zn-doped Fe_3O_4 NPs are super-paramagnetic at room temperature since their remanence (magnetization value at zero field) and coercivity (the field strength required to bring the material back to zero magnetization) is negligible in absence of an external magnetic field (inset in Figure 4). That is to say that each particle is a single magnetic domain and thermal energy can overcome anisotropy energy barrier for spin reversal (15).

One of the parameters calculable by magnetization curves is magnetic particle's size or magnetic domain size which is calculated using Eq. (4):

$$\mathbf{D_m = [18k_BT/\pi\rho \times \chi_i/M_s^2]^{1/3}} \quad (4)$$

Where; ρ is Fe_3O_4 particles density (5.18 g/cm^3), k_B is the Boltzmann constant and T is the absolute temperature (300K) (16).

As demonstrated in Table 3. particles size calculated by Eq.(4). is smaller than that calculated by TEM technique (Table 2). This difference is attributed to presence of the canted spins in the surface layers due to decrease in the exchange coupling, which leads to magnetically dead surface layers formation (5).

One of the important effects of doping on magnetite NPs magnetic properties is saturation magnetization change (M_s) whose trend is shown in Figure 5. To demonstrate M_s change more conspicuously, magnet-ization curves have been normalized in $H \geq 0$ range using M_s value at x=0 (70 emu/g).

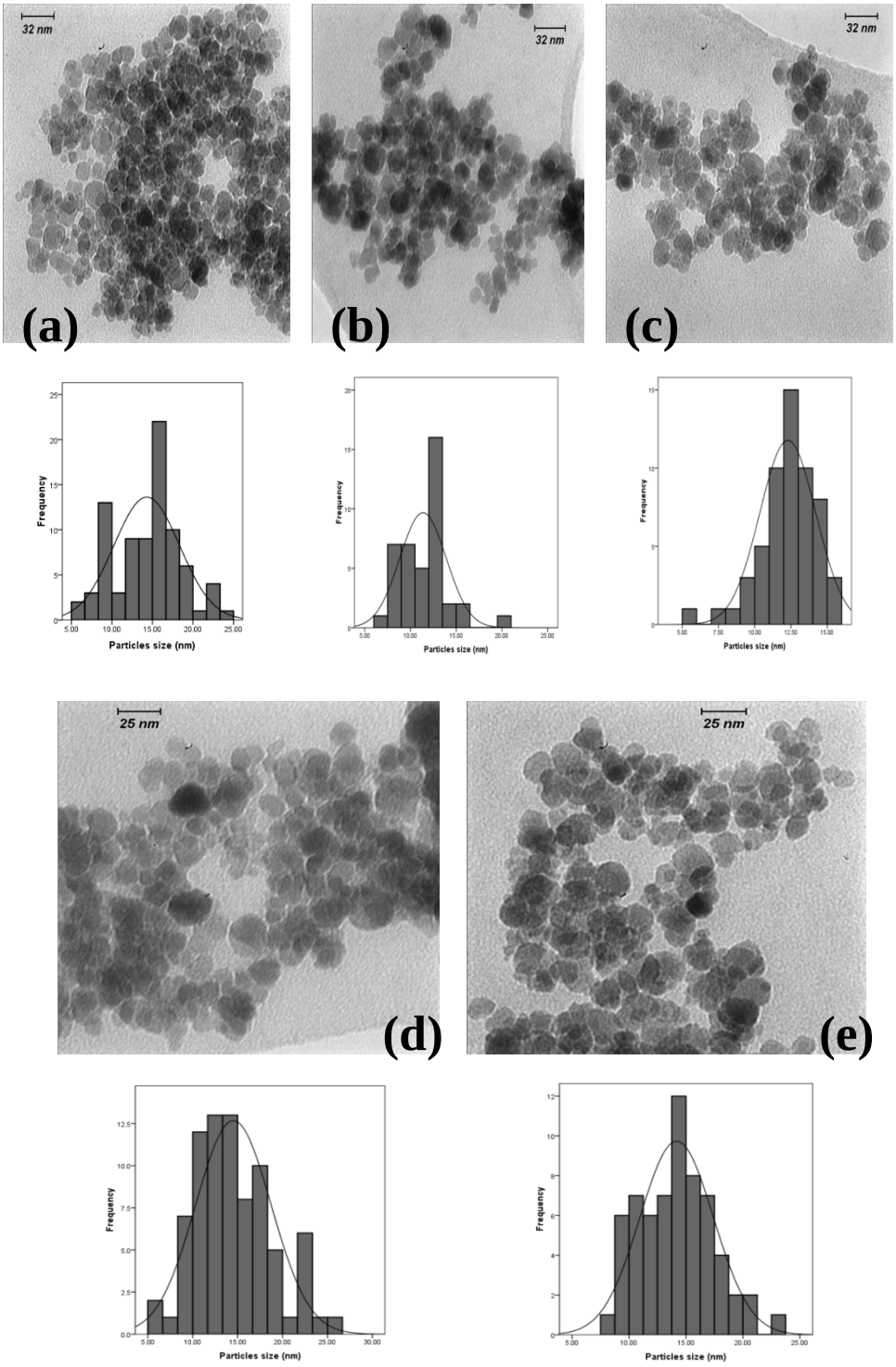

Figure 3. TEM images with size distribution histograms of $Zn_xFe_{3-x}O_4$ NPs with (a) x=0, (b) x=0.025, (c) x=0.05, (d) x=0.075 and (e) x=0.125.

Table 2. Average size of the nanoparticles obtained from TEM images.

Sampl	*X=0*	X=0.025	X=0.05	X=0.075	X=0. 125
D_{TEM} **(nm)**	14.92	11.37	12.28	14.53	14.18

Two factors can explain the above-mentioned change:

1. The first factor is the particles magnetic properties dependency on their size. With decrease in particles size, because of increase of their surface to volume ratio, the contribution to the magnetism of the NPs from the dead surface layers would be more than from inside part, which has ferro-magnetic ordering.

So due to dominant role of the dead surface layers in the particle total magnetic property, the smaller the particle size, the less the saturation magnetization (16).

Table 3. Magnetic parameters obtained from VSM analysis.

sample	M_s **(emu/g)**	M_r **(emu/g)**	H_c **(Oe)**	χ_i **(emu/g Oe)**	D_m **(nm)**
x=0	70	1.11	5	0.1971	12.25
x=0.025	67	0.79	6.23	0.1238	10.80
x=0.075	74.60	0.82	6.44	0.1337	11
x=0.1	72.12	0.41	3.03	0.1485	13.08
x=0.125	72.20	0.65	5.36	0.1264	11.10

2. The second factor is the doping effect on the ion occupation status in tetrahedral (A) and octahedral (B) sites and consequently on exchange interactions in magnetite. In this regard, recent studies have revealed that doping replaces Fe^{3+} ions with Zn^{2+} in A-site but no Zn^{2+} doping occurs in B-site (8, 9). So, it might be predicted that when Fe^{3+} ions are replaced with Zn^{2+} in A-site, the same number of Fe^{2+} ions are turned into Fe^{3+} ions through electron emission to retrieve crystal electric neutrality. In this case, M_s

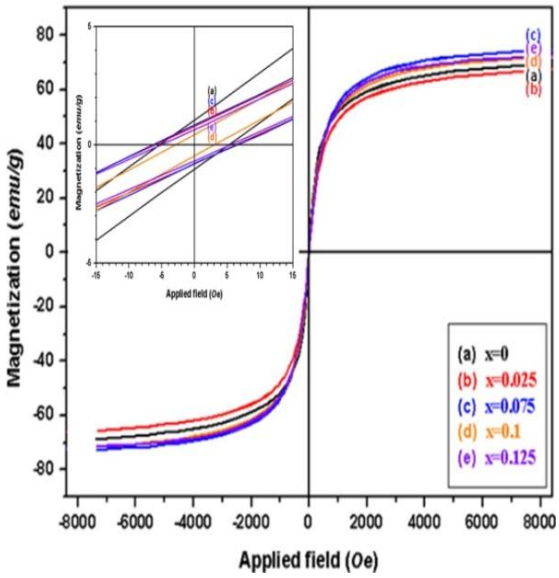

Figure 4. M-H curves of $Zn_xFe_{3-x}O_4$ nanoparticles with various Zn^{2+} values in room temperature (The inset demonstrates the enlarged curves from -15 to15 Oe).

value varies according to resultant Fe^{3+} ions spin direction in B-site (7). Generally, co-occurrence of two indirect exchange interactions in pure Fe_3O_4 (superexchange interaction between Fe^{3+} ions in tetrahedral and octahedral sites and double exchange interaction between Fe^{3+} and Fe^{2+} ions in octahedral sites) leads to antiferromagnetic orientation of tetrahedral and octahedral magnetic sub-lattice while each sub-lattice's internal magnetic arrangement is ferromagnetic. Due to this magnetic arrangement, magnetic shares of Fe^{3+} ions in A and B sites neutralize each other and only unpaired moments of Fe^{2+} ions in B-site determine the total magnetization (17). As Zn doping is added to the structure, Zn doping percent is initially low. So, Fe^{2+} ions are turned to Fe^{3+} ions, keeping their initial spin orientation. This leads to initial increase of M_s value. As Zn value increases, superexchange intera-ctions overcome double exchange intera-ctions and a number of the obtained Fe^{3+} ions are arranged in an anti- parallel orientation to the other B-site ions. This orientation decreases M_s value (7). Consequently, simultaneous effect of the mentioned

factors- crystal size end exchange interactions causes change in the saturation magnetization showed in Figure 5.

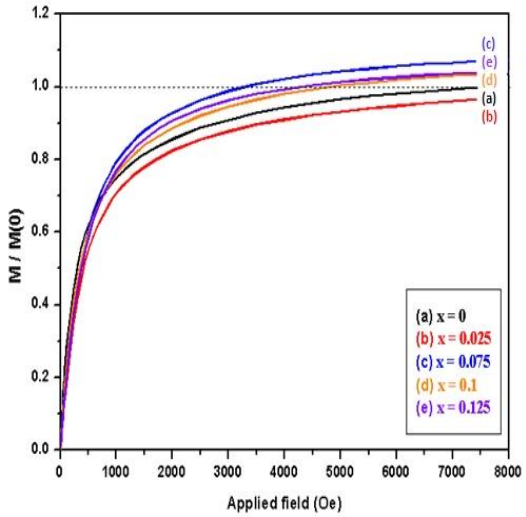

Figure 5. Magnetization curves normalized by M (0) (M_s value of the pure sample(x=0).

FT-IR analysis

Figure 6 demonstrates the FT-IR spectrum of $Zn_xFe_{3-x}O_4$ (x=0-0.125) nanoparticles. In the pure sample (x=0) spectrum, presence of absorption bands at 425, 591 and 624 cm^{-1} wavenumbers- associated with Fe-O stretching vibrations of Fe^{2+} and Fe^{3+} ions in octahedral sites and those of Fe^{3+} ions in tetrahedral sites- confirm Fe_3O_4 structure formation (18).

With the addition of impurities, zinc, despite the presence of all pure Fe_3O_4 absorption bands, as already mentioned, due to conversion of Fe^{2+} ions to Fe^{3+} ions in octahedral sites and changes in the properties of the created bonds between Fe^{3+} ions and oxygen ions, the absorption peaks of this bond shift in the FTIR spectra.

The shifting happening at the wavelength range of 578-591 cm^{-1} is clearly recognizable in the magnified Figure 6. at 400-1000 cm^{-1} range (Figure 7).

In all FTIR spectrums demonstrated in Figure 6 two absorption bands centered at 1624 and 3432 cm^{-1} can also be seen which are related to the O-H vibrations of the free water molecules and adsorbed water on samples' surface (11).

It is worth mentioning that in these spectrums, absorption bands of the Zn-O bond vibrations caused by presence of Zn^{2+} ions in Fe_3O_4 crystal lattice are invisible due to their overlapping with Fe-O vibrations absorption peaks at 425 cm^{-1} region.

Optical properties analysis

Samples UV-Vis absorption spectrums were measured to investigate Zn-doping effect on magnetite NPs optical properties such as optical absorption and band gap (Figure 8). Having added 2% Zn doping, sharp absorption edges appear in this region due to

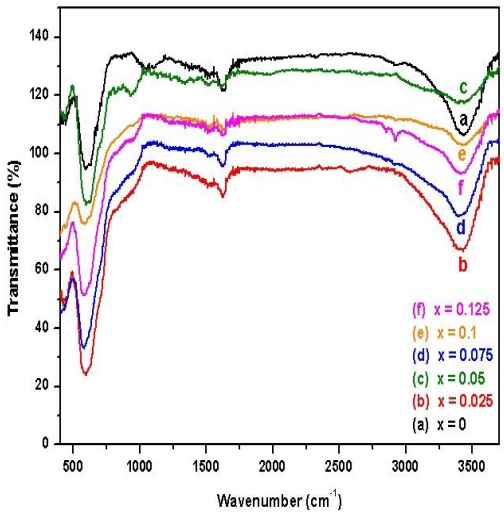

Figure 6. FTIR spectrums of the $Zn_xFe_{3-x}O_4$ ($0 \leq x \leq 0.125$) nanoparticles.

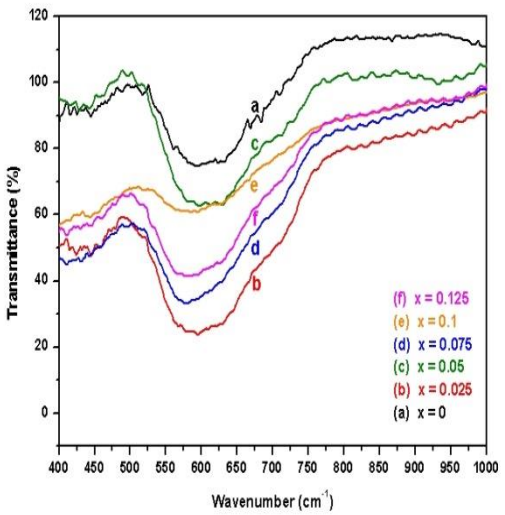

Figure 7. Magnified FTIR spectrums at 400-1000 cm^{-1} range.

light absorption and scattering by nano-particles. As demonstrated, pure Fe_3O_4 NPs do not reveal sharp absorption edges in UV region. As doping increases, optical absorption decreases. So, doping increase leads to absorption decrease and or increases nanoparticles optical transmittance which reflects Zn incorporation in Fe_3O_4 lattice.

Indirect band gap of the $Zn_xFe_{3-x}O_4$ (x=0-0.125) nanoparticles are calculated by Tauc equation Eq. (5):

$$\alpha h\nu = A\,(h\nu - E_g)^2 \qquad (5)$$

Where α is the absorption coefficient, A is a constant, h is Planck's constant, ν is the photon frequency and E_g is the energy (19).

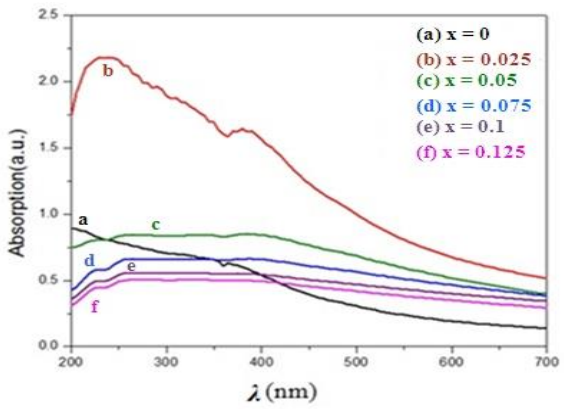

Figure 8. UV-Vis absorption spectrums of $Zn_xFe_{3-x}O_4$ (x=0-0.125) nanoparticles.

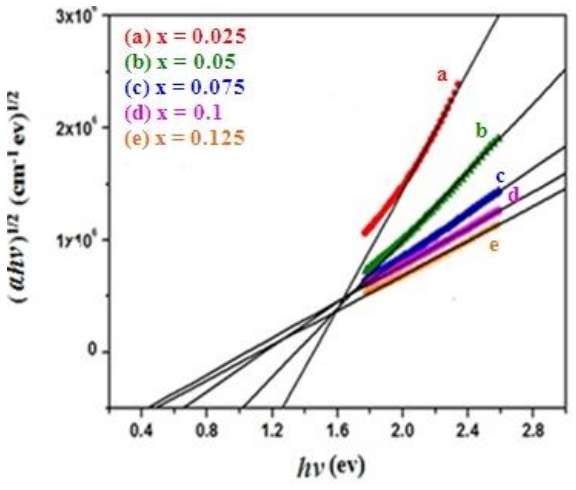

Figure 9. Optical band gap determination of samples using Tauc plots**.**

In Tauc equation; when $\alpha h\nu$=0, $h\nu$= Eg. So; Eg might be calculated by plotting a diagram of $(\alpha h\nu)^{1/2}$ versus $h\nu$ and then extrapolating their linear region (Figure 9). Band gap studies reveal that E_g value in Zn-doped Fe_3O_4 nanoparticles is higher that of pure Fe_3O_4. Based on literature, indirect band gap of Fe_3O_4 is 0.1 eV (20). As doping percent increases, indirect band gap value decreases from 1.26 eV in x=0.025 to 0.43 eV in x=0.125. This may be ascribed to the fact that new defect are introduced after substitution of Zn by Fe atoms in order to electro negativity and ionic radius difference between Zn and Fe. Moreover, there are more electrons contributed by Zn dopant due to lower electron affinity of Zn compared to Fe, (Zn=0 Kj/mol^{-1}, Fe=15 Kj/mol^{-1}) which take up the energy levels location in the bottom of the conduction band. The valence electrons require extra energy to be excited to higher energy states in the conduction band.

Conclusion

This study aims at investigating Zn-doping effects on structural, magnetic and optical properties of magnetite NPs. Based on the obtained results, in XRD patterns of all samples, magnetite pure phase formation with cubic inverse spinel structure was recognized without any secondary phase of Zn compounds. Two important effects of doping on structural properties are lattice constant increase and crystal order decrease, which were proved based on peak shift toward smaller angles and diffraction peaks intensity decrease, respectively.

Magnetic investigations on the samples reveal the formation of superparamagnetic structures with high saturation magn-etization with a maximum level of 74.60 emu/g in x=0.075. Saturation magnetization changes were explained based on

doping effects on particles crystal size and ions arrangements in tetrahedral and octahedral sites.

Optical studies revealed Fe_3O_4 nanoparticles' band gap increase due to Zn doping. As doping percent increases, band gap value decreases from 1.26 eV to 0.43 eV. It is believed that the prepared nano-composite with its magnetic potential can be considered for different biomedical and biosensing application.

Acknowledgments

This work was funded by Ferdowsi University of Mashhad, Mashhad, Iran.

References

1. Gao J, Gu H, Xu B. multifunctional magnetic nanoparticles: design, synthesis and biomedical application. Acc Chem Res. 2009; 42(8): 1097-1107.
2. Pu Y, Tao X, Zeng X, Le Y, Chen JF. Synthesis of Co–Cu–Zn doped Fe3O4 nanoparticles with tunable morphology and magnetic properties. J Magn Magn Mater. 2010; 322(14): 1985-1990.
3. Karaagac O, Kockar H, Beyaz S, Tanrisever T. A simple way to synthesize superparamagnetic iron oxide nanoparticles in air atmosphere: iron ion concentration effect. IEEE Trans Magn. 2010; 46(12): 3978-3983.
4. Zheng Y, Cheng Y, Bao F. Wang Y. Synthesis and magnetic properties of Fe_3O_4 nanoparticles. Mater Res Bull. 2006; 41(3): 525-529.
5. Ozkaya T, Toprak MS, Baykal A, Kavas H, Köseoglu Y, Aktas B. Synthesis of Fe_3O_4 nanoparticles at 100 °C and its magnetic characterization. J Alloy Compd. 2009; 472(1-2): 18-23.
6. Mohapatra M, Pandey B, Upadhyay Ch, Anand S, Das RP ,Verma HC. Effect of Ni doping on the properties of fine magnetite particles. J Magn Magn Mater. 2005; 295(1): 44-50.
7. Liu J, Bin Y. Matsuo M. Magnetic behavior of Zn-Doped Fe_3O_4 nanoparticles estimated in terms of crystal domain size. J Phys Chem C. 2012; 116(1): 134-143.
8. Pool VL, Klem MT, Holroyd J, Harris T, Arenholz E, Young M, et al. Site determination of Zn doping in protein encapsulated $Zn_xFe_{3-x}O_4$ nanoparticles. J Appl Phys. 2009; 105(7): 515-517.
9. Pool VL, Klem MT, Chorney CL, Arenholz EA, Idzerda YU. Enhanced magnetism of Fe_3O_4 nanoparticles with Ga doping. J Appl Phys. 2011; 109(7): 529-531.
10. Faraji M, Yamini Y, Rezaee M. Magnetic nanoparticles: synthesis, stabilization, functionalization, characterization and applications. J Iran Chem Soc. 2010; 7(1): 1-37.
11. Haw CY, Chia CH, Zakaria S, Mohamed F, Radiman S, Teh CH, et al. Morphological studies of randomized dispersion magnetite nanoclusters coated with silica. Ceram Int. 2011; 37(2): 451-464.
12. Wu S, Sun A, Zhai F, Wang J, Xu W, Zhang Q, et al. Fe_3O_4 magnetic nanoparticles synthesis from tailings by ultrasonic chemical co-precipitation. Mater Lett. 2011; 65(12): 1882-1884.
13. Mohammad-Beigi H, Yaghmaei S, Roostaazad R, Bardania H, Arpanaei A. Effect of pH, citrate treatment and silane-coupling agent concentration on the magnetic, structural and surface properties of functionalized silica-coated iron oxide nanocomposite particles. Physica E. 2011; 44(3): 618-627.
14. Klug HP, Alexander LE. X-ray diffraction procedure for polycrystalline and amorphous materials. New York: Jon Wiley; 1974.
15. Mo Z, Zhang C, Guo R, Meng S, Zhang J. Synthesis of Fe_3O_4 Nanoparticles Using Controlled Ammonia Vapor Diffusion under Ultrasonic Irradiation. Ind Eng Chem Res. 2011; 50(6): 3534-3539.
16. Massart R. Preparation of aqueous magnetic liquids in alkaline and acidic media. IEEE Trans Magn. 1981; 17(2): 1247-1248.
17. Dionne GF. Magnetic Oxides. New York: Springer; 2009.
18. Jitianu A, Raileanu M, Crisan M, Predoi D, Jitianu M, Stanciu L, et al. Fe_3O_4–SiO_2 nanocomposites obtained via alkoxide and

colloidal route. J Sol-Gel Sci Techn. 2006; 40(2-3): 317-323.

19. Koteeswara Reddy N, Ramakrishna Reddy KT. Optical behavior of sprayed tin sulphide thin films. Mater Res Bull. 2006; 41(2): 414-422.
20. Cabot A, Puntes VF, Shevchenko E, Yin Y, Balcells L, Marcus MA, et al. Vacancy Coalescence during
21. Oxidation of Iron Nanoparticles. J Am Chem Soc. 2007; 129 (34): 10358-10360.